Int. J. Electrochem. Sci., 12 **(2017)** 11818 – 11832, doi: 10.20964/2017.12.24

International Journal of
ELECTROCHEMICAL
SCIENCE
www.electrochemsci.org

Preparation of 3D Au NPs-poly-L-glutamate/graphene Nanocomposite Modified Electrode for Sensing of Bisphenol A

Yuli Wei[1,2], *Huihui An* [1], *Wu Yang*[1,*], *Hao Guo*[1]

[1] College of Chemistry and Chemical Engineering, Key Lab of Bioelectrochemistry and Environmental Analysis of Gansu Province, Northwest Normal University, Lanzhou 730070, China
[2] Lanzhou Petrochemical Research Center, Petrochemical Research Institute, PetroChina, Lanzhou 730060, P. R. China
[*]E-mail: xbsfda123@126.com

Received: 3 March 2017 / *Accepted:* 29 June 2017 / *Published:* 12 November 2017

In this work, a simple, sensitive and rapid electrochemical sensor for bisphenol A determination based on a 3D Au NPs-poly-L-glutamate/graphene nanocomposite was proposed and the structures of the nanocomposite were characterized by scanning electron microscopy (SEM), Fourier transform infrared spectroscopic (FTIR) and X-ray diffraction (XRD). The electrochemical behaviors of bisphenol A on the nanocomposite GCE were investigated by cyclic voltammetry (CV) and differential pulse voltammetry (DPV). In the potential range of 0.0 ~ 1.0 V, an irreversible oxidation peak appeared on the modified electrode in 0.1 mol L^{-1} phosphate buffer solution (pH = 6.0). Under the optimum conditions, the anode peak current of bisphenol A increased linearly with the its concentration in the ranges from 0.009 μmol L^{-1} to 0.1 μmol L^{-1} and 0.1 μmol L^{-1} to 1.0 μmol $L^{-1}$with the detection limit down to 3×10^{-10} mol L^{-1} (S/N = 3) and the corresponding linear regression equations were *Ipa*(μA)= − 0.1129 *C* (μmol L^{-1}) + 0.5532 (N = 6, R^2 = 0.9057) and *Ipa*(μA) = − 0.05970 *C* (μmol L^{-1}) + 0.02182 (N = 5, R^2 = 0.9950) respectively. The proposed method was successfully used for the determination of bisphenol A content in wastewater and milk samples, and the recoveries were in the range from 98.10% to 104.9%.

Keywords: bisphenol A, electrochemistry, grapheme, L-glutamic acid, sensors

1. INTRODUCTION

Bisphenol A (BPA, 2, 2-bis(4-hydroxyphenyl) propane), an important chemical industrial material, is widely used for the production of epoxy resins and polycarbonate plastics[1,2]. However, as an environmental endocrine, BPA may cause many diseases, including diabetes, heart disease, prostate cancer, breast cancer and other hormone-related cancers[1,3,4], which seriously threaten to the

human health[5]. Extensive evidences have indicated that BPA has an acute toxicity to aquatic organisms in freshwater and marine environments in the range of 1–10 μg mL^{-1} and can induce feminization during the gonadal ontogeny of fishes, reptiles, and birds. Because of the wide dispersive use, the possibility of environmental contamination by BPA is increasing, which has fueled the greatest concern and controversy in the past decade[6]. So, to develop sensitive detection methods for BPA has become one of the most magnetic subjects in analytical chemistry.

To date, many analytical technologies have been proposed to detect BPA, such as fluorescence (FL)[7-10], CE[10,12], CL[13,14], ECL[15], HPLC[16], LC–MS[17], GC[18], GC–MS[19]. Although these methods are effective and sensitive, but certain disadvantages such as time-consuming, complicated pretreatment and expensiveness restrict their wide applications. So, it is still an enormous challenge to develop operationally simple and highly selective methods for BPA determination. As a result, some new analytical methods, including electrochemistry [20, 21] and immunoassay [21, 23] have been developed for the selective detection of BPA.

Varieties of nanomaterials including gold nanoparticles (Au NPs)[24], carbon nanotubes[25] and graphene [26-33] have been certified to be excellent carriers to improve the sensitivity of the sensors. Among them, graphene, a two-dimensional (2-D) sheet of carbon atoms in a hexagonal configuration with carbon atoms bonded by sp^2 orbital, the basic building block for all other dimensional carbon materials, has attracted great interest of physicists, chemists and materials scientists [34]. It is an exciting material which broadens the horizons of materials science. Recently it has been utilized widely in chemical and electrochemical fields, because of its excellent electrical conductivity, low cost, large theoretical specific surface area and excellent biocompatibility. These unusual electronic properties make it ideal for the designing for nanoelectronic applications [35-37]. The applications of graphene in the fields of electrochemical sensors and biosensor had been reviewed [34]. At present, some reports about the determination of the environmental pollutants based on the graphene modified electrode, for example, hydroquinone and catechol [38, 39], 4-nonylphenol[40], and so on, have also been published. Generally, the modified electrodes based on the graphene nanocomposites can enhance the detection sensitivity and improve reversibility because of its unique nanostructure and extraordinary properties[6,36-41]. Furthermore, graphene can be conveniently produced using graphite, which is cheap and accessible.

Au nanoparticles (Au NPs) have also attracted considerable attentions in the fields of electronics, catalysis and biosensors because of their high specific surface area, excellent catalytic properties, fast electron transfer rate and enhancing electrode conductivity. Recently, a comprehensive and detailed review about the preparation and application of gold nanoparticles in the fields of chemical and biological sensings had been reported by Saha et al.[6,42] Gold nanoparticles possess many distinct physical and chemical properties, which make them particularly attractive for the fabrication of novel electrochemical sensors and biosensors[6]. Furthermore, gold nanoparticles dotted graphene (GNPs/GR) as enhanced sensing material for fabricating electrochemical sensors have received increased attention, because this kind of nanomaterial film may generate synergistic effects on electrochemical properties of the sensors and thus enhance the sensitivity of the sensors[43,28].

L-glutamic acid is one of the 20 common amino acids, and can be easily electropolymerized to form poly-glutamic acid (PGA)[44] and the resultant polymer is size-controlled[45]. And L-glutamic

acid polymer still has many other merits, such as good stability, high selectivity and sensitivity, simple operation etc., which are useful for electrochemical applications. The protonated cationic groups on the electrode surface are available when L-glutamic acid is used as a doping agent to modify the electrode, which is advantageous for forming stable composite with negatively charged Au nanoparticles through an electrostatic interaction. The composites of Au NPs and poly-glutamic acid can efficiently improve the conductivity of the modified electrode and enhance their electrocatalytic properties, thereby improve the sensitivity and selectivity of the determination.

As part of systematical studies on electrochemical and biosensors[6,37,41], in this present paper, we proposed a simple chemical procedure to fabricate a sensitively and rapidly responded electrochemical sensor for BPA detection based on the 3D Au NPs-poly-L-glutamate/graphene nanocomposite modified electrode. The sensor showed high sensitivity, good selectivity and excellent long-term stability.

2. EXPERIMENTAL

2.1. Instruments and reagents

All electrochemical measurements were performed on a CHI660e electrochemical workstation (Chenhua Instrument Shanghai, China) with a conventional three-electrode cell consisting of a bare or modified electrode as working electrode, a platinum wire and a saturated calomel electrode as auxiliary and reference electrodes, respectively. The electrochemical impedance spectroscopy measurements were performed on a VMP2 multi-channel potentiostats (Echem Nano Tech Services, India). A JSM-6701F field emission scanning electron microscope (SEM, Japanese Electron Optics Company, Japan) was used for morphology characterization of the modified electrodes. A JEM-1200EX transmission electron microscopy(JOEL, Japan) was applied to observed the microstructures of the samples under an acceleration voltage of 80 kV. The attenuated total reflectance Fourier transform infrared spectra(ATR FT-IR) were collected by using a Nicolet NEXUS 670 FT-IR single-beam spectrometer (USA) with a 4 cm^{-1} resolution maintaining constant contact pressure between the Ge crystal and the specimens. XRD patterns were obtained with a PANalytical X'Pert/PRO diffractometer(Netherland) in the reflection mode using CuKa radiation source with a resolution of 0.02^o and scanning speed of 0.5^o min^{-1}. Raman spectra were measured by a RFS/100/S Fourier transform Raman spectrometer(Bruker, Germany). A PHS-3C precision pH meter (Lei magnetic Company Shanghai, China) was employed to measure and control the pH of the solutions. H-1650 centrifuge (Hunan Instrument Laboratory Instrument Development Co., Ltd. China) was used for separation of the samples.

Natural graphite, chloroauric acid and L- glutamic acid were obtained from Qin Chemical Reagent Co., Shanghai. Bisphenol A(BPA, > 99.8%) was purchased from Aladdin Industrial Corporation. 0.1 mol L^{-1} phosphate buffer solution (PBS) was used as supporting electrolyte, which was prepared by mixing the stock solution of 0.1 mol L^{-1} NaH_2PO_4 and 0.1 mol L^{-1} Na_2HPO_4 and adjusting the pH with 0.1 mol L^{-1} H_3PO_4 or 0.1 mol L^{-1} NaOH solution. All of the other chemicals including HCl, HNO_3, H_2SO_4, NaCl, H_2O_2(30%), $KMnO_4$, sodium citrate(Na_3cit), methanol, ethanol

and acetonitrile, were of analytical reagent grade and purchased from Beijing Chemicals Factory. All solutions were prepared with double distilled water.

2.2. Synthesis of graphene oxide

Graphene oxide (GO) was prepared using a slightly modified Hummers method [46] by oxidation of the graphite powders. First, 2.0 g of graphite powder was weighed and added in a round bottom flask and then 46 ml of H_2SO_4 was added slowly. After stirring for 30 min in ice bath, 6.0 g of $KMnO_4$ was slowly added in the above mixed solution under vigorously stirring and maintaining the reaction temperature below 10 ℃. Finally the reaction mixture was kept stirring for 24 h at 35 ℃. After the reaction finished, the above paste was diluted with 50 ml of deionized water and 50 mL of H_2O_2 (30%) was added keeping vigorous stirring. After 2h, the color of the solution directly turned golden yellow. The mixture was cooled to room temperature, washed with 5% hydrochloric acid and water individually, and dried to obtain a black powder of graphene oxide.

2.3. Preparation of 3D Au NPs-PGA/GO/GCE electrochemical sensor

Gold nanoparticles were prepared by reduction of $HAuCl_4$ with Na_3Cit according to a slightly modified reference procedure[47]. The 3D Au NPs-PGA/GO/GCE electrochemical sensor was prepared in four steps[48]. Firstly, 4.0 mg of GO was dissolved into 2.0 mL double-distilled water with the aid of ultrasonic stirring for 1.0 h and the bare GCE was polished to a mirror with 0.03 mm alumina slurry, then washed successively with 1:1 HNO_3/H_2O(v/v), anhydrous alcohol and redistilled water. Secondly, 10.0 μL (2 mg ml^{-1}) GO-H_2O suspension was dropped on the fresh synthesized GCE surface and air dried. Thirdly, Au NPs and PGA was electrodeposited on the as-prepared GO/GCE electrode by CV sweeping between −0.4 V and 1.5 V for 8 cycles (0.1 mV s^{-1}) in 2 mmol L^{-1} colloidal gold and 5 mmol L^{-1} L- glutamic acid mixture solution. Finally, the electrode was rinsed with ultrapure water and nitrogen-dried. The preparation procedure was shown in Scheme 1.

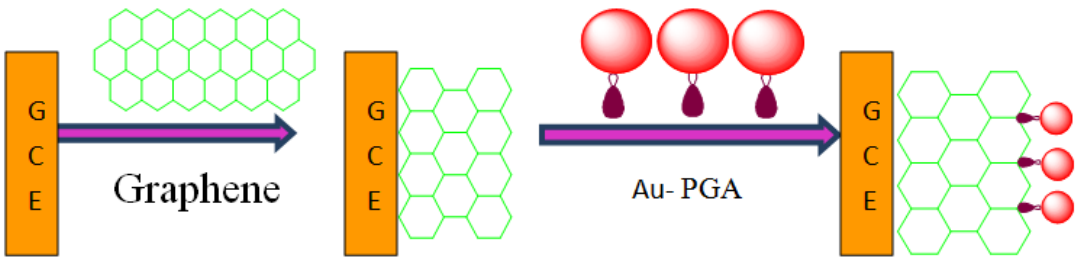

Scheme 1. The preparation procedure of the 3D Au NPs-PGA/GO/GCE.

2.4. Preparation of milk and water samples

Fresh liquid milk samples were purchased from the local supermarkets and were maintained in

their own containers under normal storage conditions. The samples are pretreated to induce protein precipitation. For this purpose, 2g milk sample was mixed with 20 ml acetonitrile and 1.0g NaCl and the mixture was ultrasonicated for 40min and centrifuged for 10min at 5000rpm. 3ml of the supernatant was transferred into a centrifuge tube and evaporated to near dryness. The residue was dissolved with 2ml methanol/water(20:80, v/v) mixed solvent to obtain test solution.

Water sample was collected from the Yellow River and wastewater treatment plant in Lanzhou respectively and the samples were filtered through 0.45μm microporous membrane to eliminate particulate matter and stored in clean glass bottles.

At last 1.0 mL of test solution was individually diluted to 10 mL with PBS buffer (0.1mol L^{-1}, pH=6.0) for electrochemical determination.

3. RESULTS AND DISCUSSION

3.1. Characterizations of GO and the modified electrode

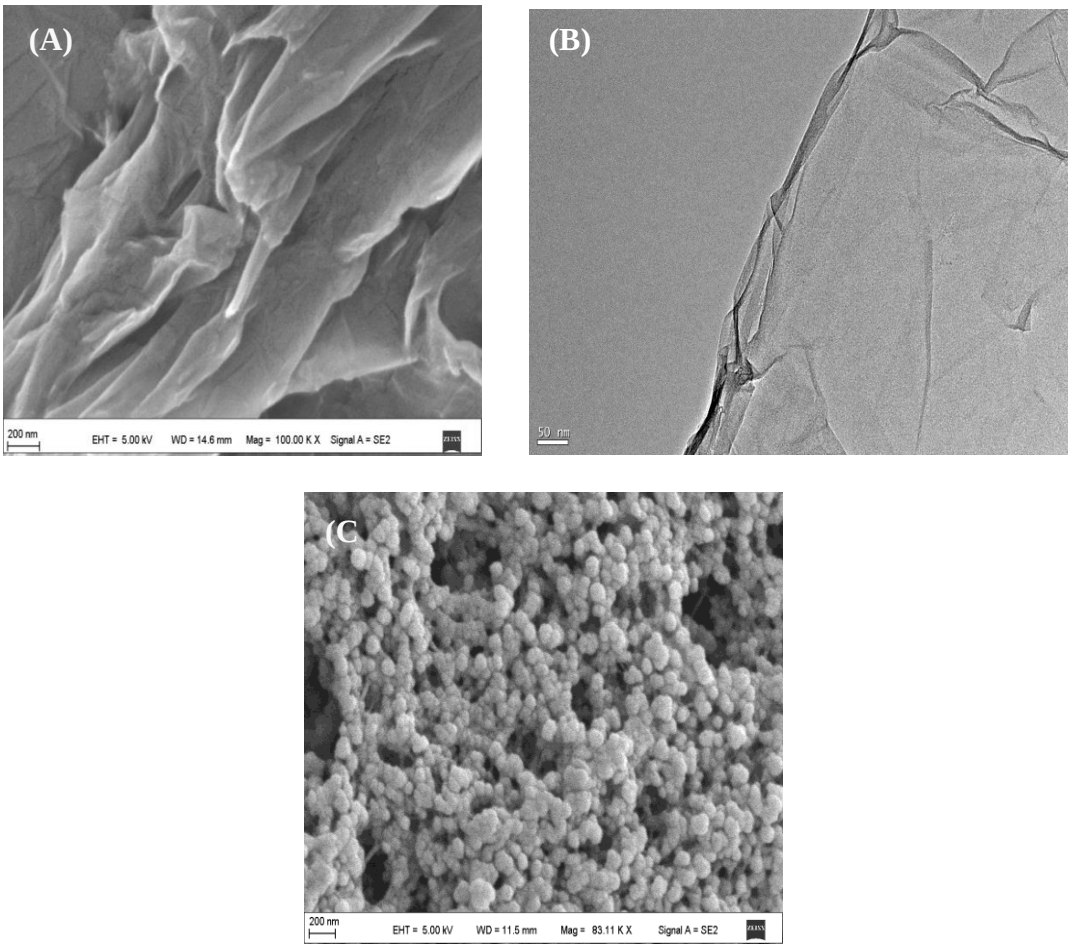

Figure 1. Morphologies of graphene oxide(GO) and the modified electrode. (A) SEM and (B) TEM images of GO, (C) SEM image of 3D Au NPs-PGA/GO/GCE.

The SEM and TEM images of GO were shown in Fig. 1A. It could be seen that GO showed a flake-like, thin wrinkled paper-like structure. Fig. 1C was SEM morphology of 3D Au NPs-PGA/GO/GCE. We could clearly observe that there were many small round Au nanoparticles well-distributed on the thin layers of graphene oxide and these results also suggested that gold nanoparticles had been successfully electroplated onto the surface of the graphene oxide modified electrode. Without PGA, Au NPs were difficult to be introduced onto the surface of GO, positive charges of PGA served as linkage agents of Au NPs and GO through a static interaction.

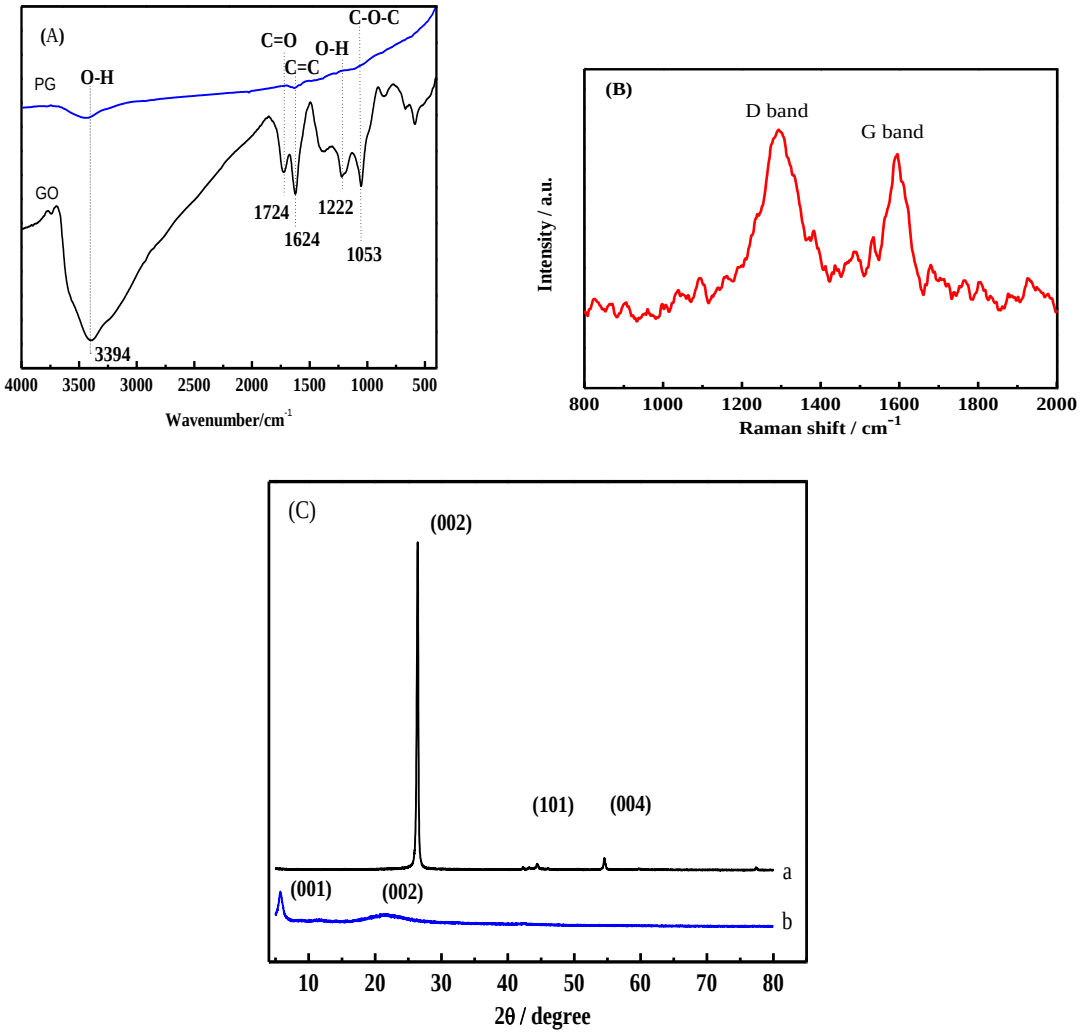

Figure 2. IR spectra(A), Raman spectra(B) and XRD pattern(C) of and graphite(PG) and graphene oxide(GO)

To get further information of the graphene structure, we also measured FT-IR spectra of graphite and GO. As shown in Fig. 2A, there was no obvious peak to be found on the pristine graphite(PG) except a broad band at 3394 cm^{-1}, which could be assigned to the O-H stretching mode of intercalated water (Fig. 2A(a)). Fig. 2A(b) was typical FT-IR spectra of GO, the bands around 3394,

1724, 1624, 1222 and 1053 cm^{-1} resulted from the oxygen-containing functional groups on GO[37]. Among them, the peaks at 1724 cm^{-1}, 1624 cm^{-1}, 1222 cm^{-1} and 1053cm^{-1} were assigned to stretching vibrations of C=O, C=C bonds, bend mode of –OH and stretching vibration of C-O-C group, respectively. After the oxidation of graphite, there were many obvious peaks detected on GO besides a broad band at 3394 cm^{-1}. Fig. 2B was Raman spectra of GO. The two peaks at 1295cm^{-1} and 1593cm^{-1} were assigned as D band and G band of GO and their intensity ratio was 1.28. These results indicated that GO had been successfully obtained.

The crystal structure and the phase purity of pristine graphite and graphene oxide were investigated by XRD, and the results were shown in Fig. 2C. The (002) characteristic diffraction peak of pristine graphite appeared at 26.4° (Fig. 2C(a)) and a very intense and sharp basal reflection indicated the highly crystalline nature of graphite. With the further oxidation, the intensity of the (002) diffraction line gradually weakened and finally disappeared[49], another new diffraction peak was found at 5.74°, which was ascribed to the (001) peak of graphene oxide (Fig. 2C(b)). In addition, no other impurities could be founded from the XRD image of GO, revealing that the resulting GO product was well crystallized and the purity was very high.

For further characterization of the modified electrodes, the electrochemical impedance spectroscopy (EIS) was recorded in the frequency range from 1 to 10^5 Hz at the formal potential of 0.2 V. As we know, the semicircle diameter in EIS equals the interface electron-transfer resistance (Ret), which controls the electron-transfer kinetics of the redox probe at the electrode interface[50]. Fig. 3 showed NY Quist diagrams of different electrodes in 5.0 mmol L^{-1} $[Fe(CN)_6]^{3-/4-}$containing 0.1 mol L^{-1} KCl. It showed that smaller well defined semi-circles at high frequency region were observed for GO/GCE and PGA/GO/GCE compared with the bare GCE and no semi-circle at high frequency region was observed for 3D Au NPs-PGA/GO/GCE electrode indicating that GO, PGA and Au NPs had a good synergy effect for electrocatalytic oxidation of BPA on the modified electrode.

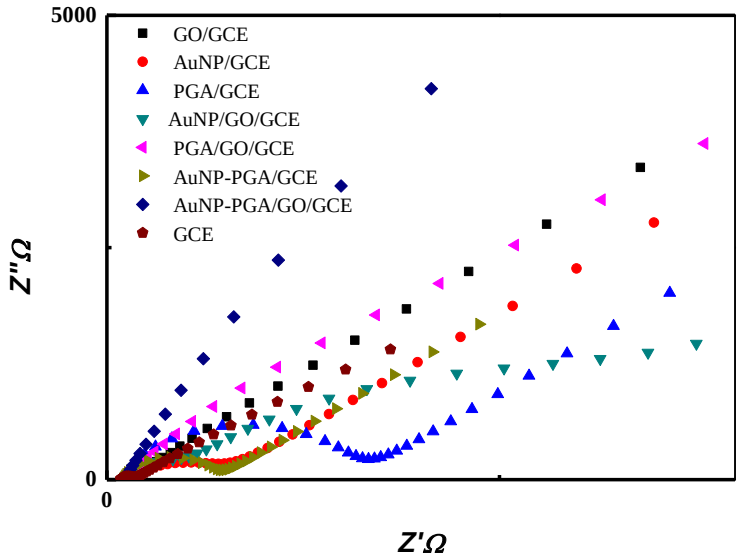

Figure 3. Electrochemical impedance spectra plots of the bare and modified electrodes in 5.0 mmol L^{-1} $[Fe(CN)6]^{3-/4-}$ containing 0.1 mol L^{-1} KCl with the frequencies swept from 4×10^3 to 0.1 Hz.

3.2. Cyclic voltammetric behaviors of BPA on different electrodes

The electrochemical behaviors of BPA at the bare GCE, GO/GCE and 3D Au NPs-PGA/GO/GCE were studied by cyclic voltammography in 0.1 mol L^{-1} PBS (pH=6.0) with 1.5×10^{-4} mol L^{-1} BPA and the results were showed in Fig. 4. At bare GCE (Fig. 4A(a)), BPA showed a wide oxidation peak and a poor electrochemical response at 0.554 V, which exhibited that the direct electron transfer of BPA on bare GCE was very slow. In addition, no reduction peak was found in the reverse scan, indicating that the electrochemical reaction was a completely irreversible process. At the GO/GCE (Fig. 4A(b)), the oxidation current increased greatly and the potential shifted positively to 0.593 V, which could be ascribed to the large specific surface area and high conductivity of GO. At the Au NPs-PGA/GO/GCE (Fig. 4A(c)), a pair of unsymmetrical redox peaks were observed. An oxidation peak and a reduction peak respectively at 0.607 and 0.516 V resulted from the oxidation of BPA and the reduction of PGA bonded Au NPs. However, the anodic peak of Au NPs was not observed, which was advantageous to determine BPA without any interference. Compared with bare GCE, the obvious peak current enhancement was undoubtedly attributed to the synergistic effect of the Au NPs-PGA/GO nanocomposite, which indicated that Au NPs-PGA/GO/GCE showed excellent electrocatalytic ability to the electrochemical oxidation of BPA.

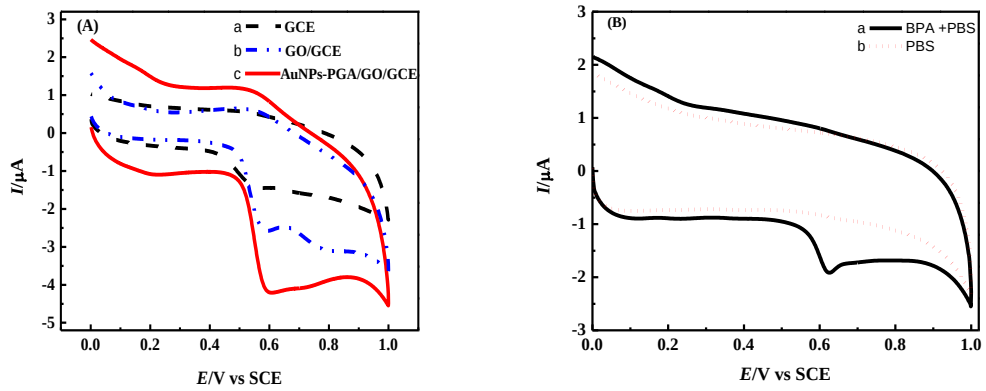

Figure 4. Cyclic voltammograms(A) of 1.5×10^{-4} mol L^{-1} BPA at bare GCE(a), GO/GCE(b), 3D Au NPs-PGA/GO/GCE (c) in 0.1 mol L^{-1} PBS (*pH*=6.0); cyclic voltammograms(B) of Au NPs-PGA/GO/GCE modified electrode in the 0.1 mol L^{-1} PBS solution(pH = 6.0) with 1.5×10^{-4} mol L^{-1} BPA (a) and without BPA(b).

Fig. 4B were the cyclic voltammograms of the 3D Au NPs-PGA/GO/GCE in 0.1 mol L^{-1} PBS (pH=6.0) with and without 1.5×10^{-4} mol L^{-1} BPA. No peak was observed when BPA was absent in the curve b. Therefore, owing to the synergetic catalytic effect, good conductivity and the accumulation effect of 3D Au NPs-PGA/GO/GCE, the electrochemical oxidation current of BPA was remarkably enhanced on 3D Au NPs-PGA/GO/GCE, which could be used to detect the trace amount of BPA.

3.3. Optimization of the experimental conditions for BPA detection

To improve the electrochemical performance of the sensor, the influences of the experimental conditions, including the deposition cycles and scan rate in preparing of 3D Au NPs-PGA/GO/GCE,

pH value of the solutions, accumulation potentials and accumulation time had been studied detailedly and the results were shown in Fig. 5.

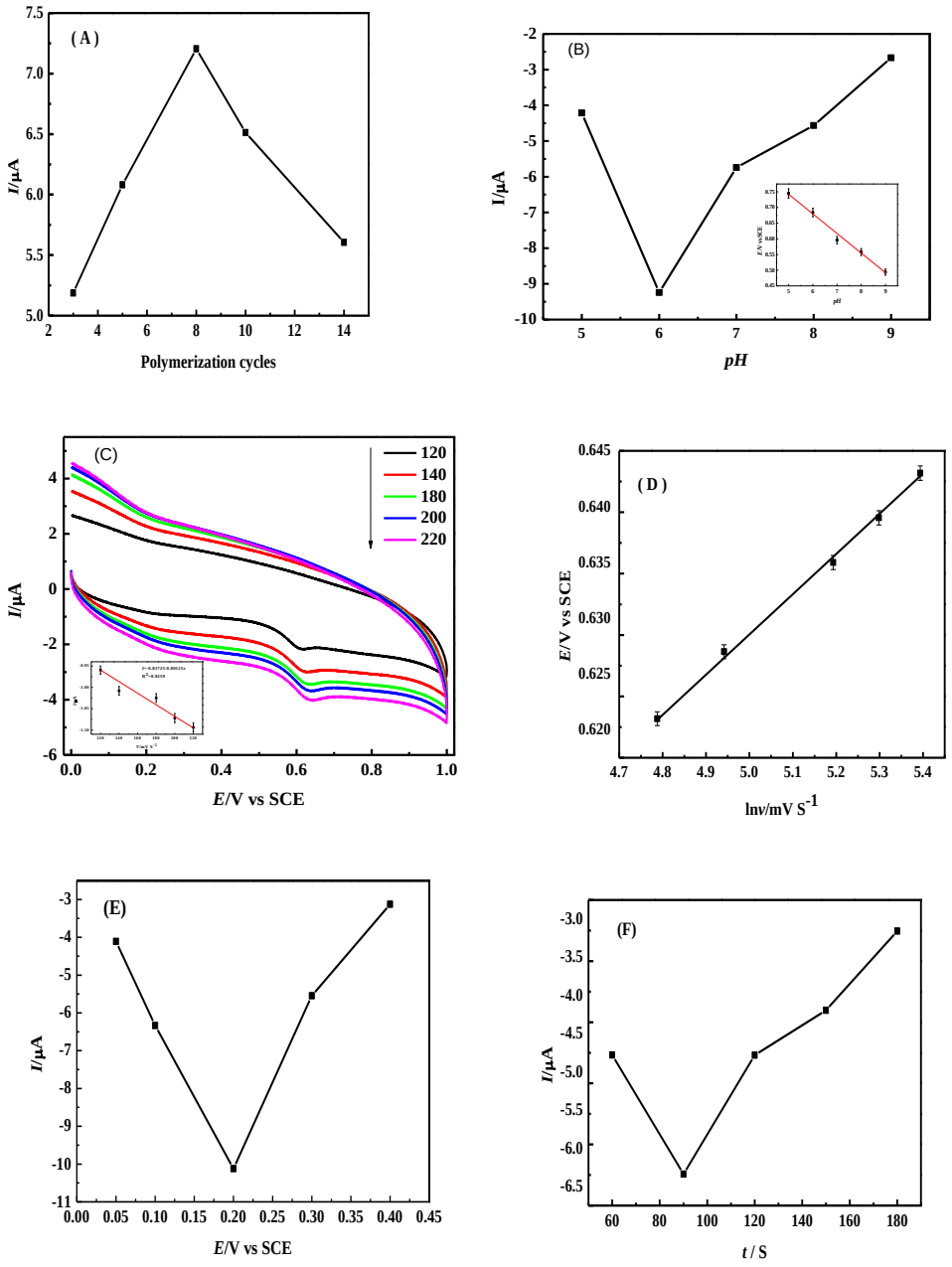

Figure 5. Effects of the experimental conditions on the peak currents of BPA in 0.1mol L^{-1} PBS buffer (pH=6.0). (A) Polymerization cycles, scanning rate: 50m V s^{-1}; (B) *pH* of the solution, scanning rate: 50m V s^{-1}, inset: dependence of the oxidation peak potentials for BPA on pH; (C) different scan rates, 120, 140, 180, 200, 220 mV s^{-1} respectively, inset: plots of peak currents vs. the scan rates; (D) relationship between the peak potential and natural logarithm of the scanning rates for BPA; (E) accumulation potential, scanning rate: 50 m V s^{-1}; (F) accumulation time, scanning rate: 50 m V s^{-1};

When the deposition potential was set in range of -0.4 ～ 1.5V, the deposition time could be controlled by the polymerized cycles. Thehighest peak current was obtained when the cycle number was 8 (Fig. 5A). pH of the solution has a considerable influence on the electrochemical behavior of BPA. With the pH increasing from 5.0 to 9.0, the peak current increased and reached a maximum at pH 6.0, and then decreased evidently(Fig. 5B). Therefore, pH 6.0 was chosen as the optimal value for the electrochemical oxidation of BPA. The relationship between the oxidation peak potential and pH value was also studied. It was found that the peak potential shifted negatively along with the pH value increasing. The relationship between the peak potentials and pH was shown in Fig. 5B(Inset), and it obeyed a linear regression equation: *Epa* (V) = 1.0587-0.0628 *pH*. According to the Nernst equation, the slope of 62.8 mV/pH demonstrated that the numbers of electrons and protons involved in the electrochemical reaction were the same.

To further understand the characteristics of 3D Au NPs-PGA/GO/GCE, the electrochemical behaviors of BPA at 3D Au NPs-PGA/GO/GCE with different scan rates were investigated. Fig. 5C showed the cyclic voltammograms of 1.5×10^{-4} mol L^{-1} BPA at 3D Au NPs-PGA/GO/GCE with different scan rates. As shown in Fig. 5C, the peak currents of BPA linearly increased with the scan rates over the range of 120 to 220 mV s^{-1} and the corresponding regression equation was *Ipa*(uA) = 0.00125 υ(mV s^{-1}) + 0.81725 with a squared correlation coefficient of 0.9259, demonstrating the electrochemical oxidation of BPA at 3D Au NPs-PGA/GO/GCE was a typical adsorption-controlled process.

Moreover, a linear relationship between *Epa* and natural logarithm of the scan rates (lnυ) was also observed(Fig. 5D). The equation was expressed as:

$$Epa\ (V) = 0.4515 + 0.0354\ln\upsilon\ (R^2=0.9973) \quad (1)$$

For a completely irreversible electrochemical process, the relationship between the oxide peak potential (*Epa*) and scan rates (υ) could be expressed by the Laviron's theory [25-27,40]:

$$Epa = E^0 + (RT/\alpha nF)\ln(RTk^0/\alpha nF) + (RT/\alpha nF)\ln\upsilon \quad (2)$$

where α is transfer coefficient, k^0 is standard rate constant of the reaction, n is electron transfer number involved in rate determining step, υ is scan rate, E^0 is formal redox potential, and R, T, F have their usual meanings[51]. According to the slope of the plot of *Epa* versus lnυ, the value of αn was calculated to be 0.73. Generally, α is assumed to be 0.5 in a completely irreversible electrode process. Thus, the electron transfer number (n) for oxidation of BPA is around 2. And the proton transfer number should also be 2 on the basis of the relationship between peak potential and pH value. Therefore, the charge transfer coefficient was calculated to be 0.37. The probable reaction of BPA on 3D Au NPs-PGA/GO/GCE was described as Scheme 2.

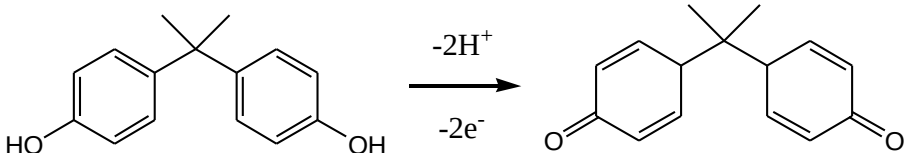

Scheme 2. Possible reaction mechanism of BPA on the Au NPs-PGA/GO/GCE

To provide a good microenvironment for the electrochemical oxidation of BPA, the accumulation potential and accumulation time were investigated by using CV in 0.1 mol L^{-1} PBS solution(pH = 6.0) containing 1.5×10^{-4} mol L^{-1} BPA. The oxidation peak current at first increased until a maximum at 0.20V and then decreased when the accumulation potential shifted from 0.2 to 1.0 V. Therefore, 0.2 V was chosen as the optimal accumulation potential(Fig. 5E). Besides, the effect of accumulation time on the peak current of BPA at accumulation potential of 0.2V was also studied. It could be obviously seen from Fig. 5F that the peak current increased as the accumulation time increased and reached the maximum value at 90 s. So in order to enhance the sensitivity and decrease detection limit, the accumulation conditions of 0.2 V and 90 s were chosen to detect BPA in the further experiments.

3.4. Electrochemical determination of BPA using differential pulse voltammetry (DPV)

The 3D Au NPs-PGA/GO/GCE was applied for sensitive BPA determination. Under the optimized conditions, the anode peak current of BPA increased with increasement of its concentration in the range from 0.009 μmol L^{-1} to 1.0 μmol L^{-1} as shown in Fig. 6A. The peak current was directly proportional to BPA concentration in the ranges of 0.009 μmol L^{-1} to 0.1 μmol L^{-1} and 0.1 μmol L^{-1} to 1.0 μmol L^{-1} and the linear regression equations were Ipa(μA)= − 0.1129 C (μmol L^{-1}) + 0.5532 (N = 6, R^2 = 0.9057) and Ipa(μA) = − 0.05970 C (μmol L^{-1}) + 0.02182 (N= 5, R^2 = 0.9950), respectively (Fig. 6B). The detection limit was calculated as 0.30 nmol L^{-1}(S/N=3), Which is lower than those of some electrochemical sensors reported recently based on nanoparticles and carbon based materials, such as cuprous oxide wrapped graphene oxide nanoparticles modified glass carbon electrode(Cu_2O-rGO/GCE)(5.3×10^{-8}M[52], multiwalled carbon nanotube and gold nanoparticle composite modified glassy carbon electrode(MWCNTs/AuNPs/GCE)(4.0×10^{-9} M)[53], multiwalled carbon nanotubes-polyethyleneimine nanocomposites modified glass carbon electrode(MWCNTs-PEI/GCE(3.3×10^{-9}M)[54], ordered mesoporous carbon CMK-3 modified nano-carbon ionic liquid paste electrode (CMK-3/nano-CILPE)(5×10^{-8}M)[55] and PtNPs/graphene–carbon nanotubes(PtNPs/rG/CNTs/GCE)(4.2×10^{-8}M)[21] or close to that of aptamer-functionalized nanoporous gold film (NPGF)(5.6×10^{-11}M)[56]. The propose method is also more sensitive than other methods reported previously, including Fe_3O_4 nanospheres/reduced graphene oxide nanocomposites based colorimetry(LOD = 5×10^{-9}M) [20], gold(III)–peroxymonocarbonate chemiluminescence(LOD=8×10^{-8}M)[13], gas chromatography coupled with nitrogen–phosphorus detection(LOD = 4.7×10^{-10}M)[18], Cd-doped ZnO quantum dots-based immunoassay(LOD = 6.17×10^{-8}M)[20] and multi-channel immunosensors (EWMI)(1.2×10^{-10}M)[23].

A comparison of this method with some electrochemical procedures reported previously was tabulated in Table 1, and it was found that the proposed procedure in this present paper had a lower detection limit.

Table 1. Comparison of Some electrochemical sensors for the detection of bisphenol A.

Electrodes	Linear range (mol L^{-1})	Detection limit (mol L^{-1})	References
Cu_2O-rGO/GCE	1.0×10^{-7}- 8.0×10^{-5}	5.3×10^{-8}	[52]
MWCNTs/AuNPs/GCE	1.0×10^{-8} – 7.0×10^{-7}	4.0×10^{-9}	[53]
MWCNTs-PEI/GCE	1.0×10^{-8}- 5.0×10^{-5}	3.3×10^{-9}	[54]
PtNPs/rG/CNTs/GCE	6.0×10^{-8} – 8.0×10^{-5}	42×10^{-8}	[21]
CMK-3/nano-CILPE	2.0×10^{-7} - 1.5×10^{-4}	5×10^{-8}	[55]
NPGF	1.0×10^{-10} - 1.0×10^{-7}	5.6×10^{-11}	[56]
3D AuNPs-PGA/GO/GCE	9.0×10^{-9} - 1.0×10^{-6}	3×10^{-10}	This work

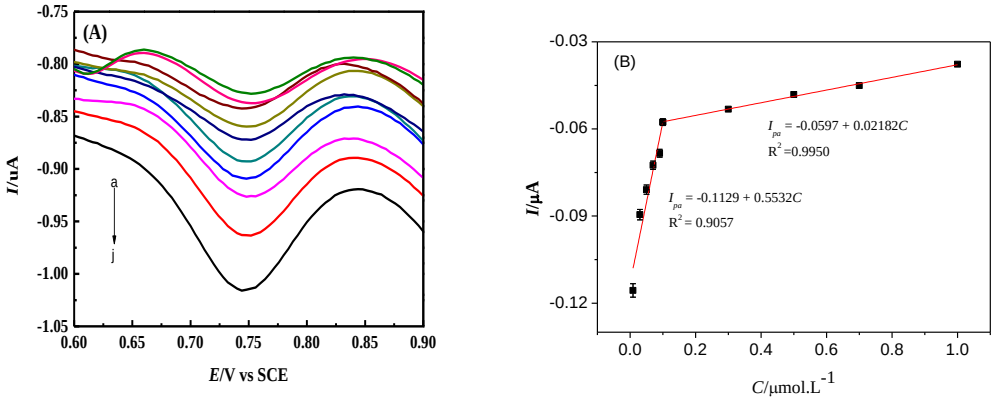

Figure 6. (A) Differential pulse voltammograms of BPA with concentrations increasing from a to j: 0.009, 0.03, 0.05, 0.07, 0.09, 0.1, 0.3, 0.5, 0.7, 1 μmol L^{-1}. (B) The relationship of the oxidation peak current (Ipa) with the concentration of BPA.

3.5. Reproducibility and stability of the modified electrode

In order to evaluate the precision of the proposed method, the repeatability of the 3D Au NPs-PGA/GO/GCE was studied by determining a 0.6 μmol.L^{-1} BPA solution for 5 times successively with the same electrode. The results showed that the electrode possessed a satisfactory repeatability and relative standard deviation (RSD) was 3.2%. The long term stability of the 3D Au NPs-PGA/GO/GCE was also investigated by keeping the modified electrode at room temperature for 15 days, 94% of the initial current value was maintained, which indicated that the 3D Au NPs-PGA/GO/GCE was stable for electrochemical application.

3.6. Interference of coexisting substances

To demonstrate the selectivity of the electrochemical sensor, the influences of some possible interfering substances were examined in 0.1mol L^{-1} PBS solution (pH 6.0). The oxidation peak currents of 6.0×10^{-6} mol L^{-1} BPA in the absence and presence of different concentrations of interferon's were measured. It was found that 2-fold concentration of hydroquinone had no influence.

Some ions, such as 100-fold concentration of K^+, Cl^{-1}, Ca^{2+}, SO_4^{2-}, Cu^{2+}, Zn^{2+}, Mg^{2+}, NO^{3-} had no influence on BPA determination too.

3.7. Analysis of real samples

The proposed sensor was employed to *in situ* determine trace amount of BPA in wastewater and milk samples. The results were given in Table 2. It was found that the recoveries were ranged from 98.10% to 104.9%, suggesting that the 3D Au NPs-PGA/GO modified electrode was effective and feasible and it could be successfully used for the detection of BPA in real samples.

Table 2. Determination of BPA in wastewater and milk samples

Sample		Detected (μmol L^{-1})	Added (μmol L^{-1})	Found (μmol L^{-1})	Recovery (%)	RSD (n=5, %)
Wastewater	1	6.39	3	9.29	98.44	2.2
	2	7.55	3	10.76	102.8	4.3
	3	10.21	3	13.03	98.24	2.5
	4	6.68	3	10.01	104.9	3.6
Milk	5	ND	1.0	0.9956	—	
	6	ND	1.0	0.9460	—	
	7	0.5728	1.0	1.554	98.10	6.2

4. CONCLUSIONS

In this work, a 3D Au NPs-PGA/GO nanocomposites modified electrode was successfully prepared by a dropped combined electro-deposited method and used to determine BPA. The prepared electrode not only showed a high electrocatalytic activity towards the oxidation of BPA, but also had an good long-term stability and an excellent reproducibility. The sensor could be applied to determine BPA in milk and wastewater without any pretreatment possess. The practical application in determining wastewater and milk samples was satisfactory with recoveries from 98.10% to 104.9%. This method provided a promising platform for electrochemical sensing BPA in real samples..

ACKNOWLEDGMENTS
This work was supported in part by the Key Project of Science and Technology of Education Ministry (00250), National Natural Science Foundation(21665024) and Gansu Key Lab of Polymer Materials, China.

References

1. H. Sambe, K. Hoshina, K. Hosoya, J. Haginaka, *J. Chromatogr*. A, 1134(2006)16.

2. N. Huang, Liu M. L., Li H. T., Zhang Y. Y., Yao S. Z., Anal. Chim. Acta., 853(2015)249.
3. J. A. Brotons, M. F. Olea-Serrano, M. Villalobos, V. Pedraza, N. Olea, *Environ. Health Perspect.*, 103(1995)608.
4. X. Q. Wu, Z. Zhang, J. H. Li, H. Y. You, Y. B. Li, L.X. Chen, *Sens. Actuators* B, 211(2015)507
5. H. Mielke, F. Partosch, U. Gundert-Remy, *Toxicol. Lett.*,204(2011)190.
6. X. L. Niu, W. Yang, G. Y. Wang, J. Ren, H. Guo, J. Z. Gao, *Electrochim. Acta*, 98(2013)167
7. X. Wang, H. Zeng, Y. Wei, J. Lin, *Sens. Actuators* B, 114(2006)565.
8. G. A. Ibanez, G. M. Escandar, *Sensors* (Basel), 11(2011)11081.
9. J. Fan, H. Guo, G. Liu, P. Peng, *Anal. Chim. Acta*, 585(2007)134.
10. H. Z. Lu, S. F. Xu, *Biosens. Bioelectrotron*., 92(2017)147
11. S. Mei, D. Wu, M. Jiang, *Microchem. J*., 98(2011)150.
12. S. X. Zhong, S. N. Tan, L. Ge, W. Wang, *J. Chen, Talanta*, 85(2011)488.
13. C. Lu, J. G. Li, Y. Yang, Talanta, 82(2010)1576.
14. S. H. Wang, X. T. Wei, L. Y. Du, S. H. Zhuang, *Luminescence*, 20(2005)46.
15. Y. F. Zhuang, J. T. Zhang, G. P. Cao, *J. Chin. Chem. Soc.*(Peking), 55(2008)994.
16. M. F. Brugnera, M. A. G. Trindade, M. V. B. Zanoni, *Anal. Lett.*, 43(2010)2823.
17. S. N. Pedersen, C. Lindholst, *J. Chromatogr*. A, 864(1999)17.
18. H. S. Shin, C. H. Park, S. J. Park, *J. Chromatogr*. A, 912(2001)119.
19. I. Kosarac, C. Kubwabo, K. Lalonde, *J. Chromatogr.* B, 898(2012)90.
20. J. Qian, X. W. Yang, L. Jiang, *Sens. Actuators* B, 201(2014)160.
21. Z. Zheng, Y. Du, Z. Wang, *Analyst*, 138(2013)693.
22. J. Zhang, S. Q. Zhao, K. Zhang, J. Q. Zhou, *Chemosphere*, 95(2014)105.
23. X. H., Zhou, B. D. Song, H. C. Shi, L. H. Liu, H. L. Guo, M. He, *Sens. Actuators* B, 198(2014)150.
24. K. J. Huang, Y. J. Liu, Y. M. Liu, *J. Hazard. Mater.*, 276(2014)207.
25. Y. Q. Lin, K. Y. Liu, C. Y. Liu, *Electrochim. Acta*, 133(2014)492.
26. C. Wu, Q. Chen, L. Q. Li, *Electrochim. Acta*, 115(2014)434.
27. S. Jiao, J. Jin, L. Wang, *Talanta*, 122(2014)140.
28. L. Zhou, J. P. Wang, D. J. Li, *Food Chem.*, 162(2014)34.
29. Y. Liu, Y. Liu, H. B. Feng, *Biosens. Bioelectron.*, 35(2012)63.
30. S. J. Xu, Y. Liu, T. H. Wang. *Anal. Chem*., 83(2011)3817.
31. Y. Wang, Z. Chen, Y. Liu, *Nanoscale*, 5(2013)7349.
32. P. Bollella, G. Fusco, C. Tortolini, G. Sanzo, G. Favero, L. Gorton, R. Antiochia, *Biosens. Bioelectron*., 89(2017)152
33. R. Sha, S. K. Puttapati, V. VSS. Srikanth, S. Badhulika, *J. Electroanal. Chem*., 785(2017)26
34. M. Pumera, A. Ambrosi, A. Bonanni, E. L. K. Chng, H. L. Poh, *Trends Anal. Chem.*, 29(2010)954.
35. A. K. Geim, K. S. Novoselov, Nature Mater., 6(2007)183.
36. Y. Zhu, S. Murali, W. Cai, X. Li, J. W. Suk, J. R. Potts, R. S. Ruoff, *Adv. Mater*., 22(2010)3906.
37. X. L. Niu, W. Yang, J. Ren, H. Guo, S. J. Long, J. J. Chen, J. Z. Gao, *Electrochim. Acta*, 80(2012)346
38. H. S. Yin, L. Cui, Q. P. Chen, *Food Chem*., 125(2011)1097.
39. H. S. Yin, Q. M. Zhang, Y. L. Zhou, *Electrochim. Acta*, 56(2011)2748.
40. W. S. Zhou, B. Zhao, X. H. Huang, *Chin. J. Anal. Chem.*, 41(2013)675.
41. X. L. Niu, W. Yang, H. Guo, J. Ren, J. Z. Gao, *Biosens. Bioelectron*.,41(2013)225.
42. K. Saha, S. S. Agasti, C. Kim, X. Li, V. M. Rotello, *Chem. Rev.*,112(2012)2739.
43. R. Y. Li, Q. F. Xia, Z. J. Li, *Biosens. Bioelectron*., 44(2013)235.
44. M. P. N. Bui, C. A. Li, K. N. Han, X. H. Pham, G. H. Seong, Sens. Actuators B, 174(2012)318
45. A. Richard, A. Margaritis, *Crit. Rev. Biotechnol*., 21(2001)219.
46. T. Kuila, S. Bose, P. Khanra, A. K. Mishra, N. H. Kim, J. H. Lee, *Biosens. Bioelectron*., 26(2011)4637.

47. D. R. Bentley, S. Balasubramanian,H. P. Swerdlow, *Nature,* 456(2008)53.
48. L. J. Zi, J. J. Li, Y. X. Mao, R. Yang, L. B. Qu, Electrochim. Acta, 78(2012)434.
49. Y. L. Wei, F. Fang, W. Yang, H. Guo, X. L. Niu, L. J. Sun, J. Braz. Chem. Soc., 26(2015)2003
50. W. S. Zhou, C. H. Li, C. Sun, X. D. Yang, Food. Chem., 192(2016)351
52. R. G. Shi, J. Liang, Z. S. Zhao, A. F. Liu, Y. Tian, *Talanta*,169(2017)37-43
53. N. B. Messaoud, M. E. Ghica, C. Dridi, M. B. Ali, C. M. A. Brett, *Sens. Actuators B*,2017, https://doi.org/10.1016/j.carbpol.2017.03.045
54. Y. Y. Yang, H. Zhang, C. S. Huang, N. Q. Jia, *Sens. Actuators B*, 235(2016)408-413
55. Y. H. Li, X. R. Zhai, X. S. Liu, L. Wang, H. R. Liu, H. B. Wang, *Talanta*, 148(2016)362-369
56. Y. Zhu, C. Q. Zhou, X. P. Yan, Y. Yan, Q. Wang, *Anal. Chim. Acta*, 883(2015)81-89